RSC Advances

PAPER

View Article Online
View Journal | View Issue

Cite this: *RSC Adv.*, 2022, **12**, 29124

Pebax® 2533/PVDF thin film mixed matrix membranes containing MIL-101 (Fe)/GO composite for CO_2 capture

Guoqiang Li, Wojciech Kujawski,* Katarzyna Knozowska and Joanna Kujawa

MIL-101 (Fe) and MIL-GO composites were successfully synthesized and used as fillers for the preparation of Pebax® 2533/PVDF thin film MMMs for CO_2/N_2 separation. The defect-free Pebax® 2533/PVDF thin film MMMs were fabricated by casting the Pebax solution containing fillers on the PVDF support. The presence of GO nanosheets in the reaction solution did not destroy the crystal structure of MIL-101 (Fe). However, the BET surface area and total pore volume of MIL-GO decreased dramatically, comparing with MIL-101 (Fe). The incorporation of MIL-GO-2 into Pebax matrix simultaneously increased the CO_2 permeability and the CO_2/N_2 ideal selectivity of Pebax® 2533/PVDF thin film MMMs mainly owing to the porous structure of MIL-GO-2, and the tortuous diffusion pathways created by GO nanosheets. MMMs containing 9.1 wt% MIL-GO-2 exhibited the highest CO_2 permeability equal to 303 barrer (1 barrer = 10^{-10} cm^3 (STP) cm cm^{-2} s^{-1} $cmHg^{-1}$) and the highest CO_2/N_2 ideal selectivity equal to 24. Pebax-based MMMs containing composite fillers showed higher gas separation performance than the Pebax-based MMMs containing single filler (GO or MOFs). Therefore, the synthesis and utilization of 3D@2D composite filler demonstrated great potential in the preparation of high-performance MMMs for gas separation processes.

Received 14th August 2022
Accepted 4th October 2022

DOI: 10.1039/d2ra05095a

rsc.li/rsc-advances

1. Introduction

CO_2 emission has been increasing dramatically owing to the rapid industrialization and the fast development of economy in the world, which has resulted in the extreme climate and global warming.[1,2] Therefore, it is of global concern to decrease the CO_2 emission by separating CO_2 from N_2 and other gases owing to the environmental and economic incentives for the utilization of the separated CO_2.[3] Membrane technology has shown great potential in gas separation processes due to its high modularity and compactness, low energy consumption, and low operating costs.[3–5] Moreover, it is tolerable for the feed composition to change since there is no phase change or solvent regeneration process.[3]

Polymeric membranes have been widely used in gas separation processes owing to their high processability and reasonable cost of polymer materials. However, it is challenging to prepare polymeric membranes possessing the high gas separation performance owing to the trade-off relationship between the permeability and the selectivity which is represented by the Robeson upper bound.[6,7] The preparation of mixed matrix membranes (MMMs) is an effective solution to surpass the Robeson upper bound.[7] The incorporation of nanomaterials into polymeric matrix can create the additional continuous gas transport channels, resulting in the enhancement of gas separation performance of MMMs.[8] Various inorganic nanomaterials have been used as fillers in MMMs preparation, such as zeolites,[9] metal–organic frameworks (MOFs),[10] graphene oxide (GO),[11] and carbon nanotubes (CNTs).[12] Fillers refer to the inorganic materials like nanoparticles that are incorporated into MMMs in order to enhance the membrane performance.

Among various fillers used in MMMs preparation, MOFs have been intensively investigated since MOFs possess high surface area, tunable porosity and pore size, and chemical functionality.[13] MOFs can be modified with CO_2-philic chemicals, such as ionic liquids (ILs),[14] isophthalic dihydrazide (IPD),[15] and polyethyleneimine (PEI),[16] to enhance their affinity to CO_2 molecules in order to improve the CO_2 permeability and selectivity of MMMs. Chen *et al.*[14] synthesized [Bmim][NTf_2] modified MOF-801 *via* wet impregnation and prepared MMMs by incorporating the synthesized filler into polymers of intrinsic microporosity PIM-1 matrix. It was found that the CO_2 permeability of IL@MOF/PIM-5% MMMs increased by 130% and the CO_2/N_2 selectivity increased by 45%, comparing with the pristine PIM-1 membranes. The enhancement of the gas separation performance was owing to the high porosity and good CO_2 affinity of IL@MOF-801 fillers, which significantly increased the diffusion rate of CO_2. Moreover, the selectivity of MMMs increased owing to the reduction of pore volume of IL@MOF-801 composites. Shi *et al.*[15] modified zeolitic imidazolate framework (ZIF-8) nanoparticles by coating isophthalic dihydrazide (IPD) molecular layer onto their surfaces by using

Nicolaus Copernicus University in Toruń, Faculty of Chemistry, 7 Gagarina Street, Toruń 87-100, Poland. E-mail: wkujawski@umk.pl

coordination interaction. Subsequently, the modified IPD@ZIF-8 nanoparticles were incorporated into 6FDA-Durene polyimide (PI) matrix for the MMMs preparation. It was found that the modified IPD@ZIF-8 nanoparticles showed enhanced interfacial compatibility between fillers and PI matrix owing to the formed hydrogen bond. As a result, the prepared MMMs containing high loading content (45 wt%) showed high CO_2 permeability equal to 4133 barrer which increased by 154%, comparing with the pristine PI membranes. Jiao *et al.*[16] synthesized PEI modified ZIF-8 (PEI-ZIF-8) by using Hmin and PEI mixed linker. The prepared PEI-ZIF-8 was incorporated into Pebax® 1657 matrix to fabricate MMMs. It was found that the MMMs with 5 wt% PEI-ZIF-8 exhibited increased CO_2 permeance equal to 13 GPU and increased CO_2/N_2 selectivity equal to 49. The improved gas separation performance for MMMs was ascribed to the porous structure and higher affinity with CO_2 of PEI-ZIF-8, the large density of amine groups from PEI providing facilitated CO_2 transport path and the enhanced interfacial compatibility.

GO as a two-dimensional (2D) material has been used in the preparation of MMMs owing to its high aspect ratio, high mechanical and thermal properties, facile preparation, and tunable surface modification.[17] In MMMs, GO nanosheets improve the gas diffusivity selectivity by creating tortuous pathways which allow small gas molecules to transport through membranes more easily than big gas molecules.[17] Therefore, the incorporation of MOF/GO composite filler into MMMs is an effective way to enhance their gas separation performance due to the synergistic effects of MOF and GO.[17,18]

Dong *et al.*[17] synthesized ZIF-8@GO composite filler and incorporate it into Pebax matrix to prepare MMMs for gas separation. It was found that MMMs containing 6 wt% of ZIF-8@GO demonstrated the CO_2 permeability of 249 barrer and CO_2/N_2 ideal selectivity of 47.6 which are 191% and 174% higher than those of pristine Pebax membranes, respectively. Moreover, the gas separation performance of MMMs containing ZIF-8@GO is higher than that of MMMs containing ZIF-8 or GO. The enhancement of gas separation of MMMs containing ZIF-8@GO was mainly due to the synergistic effects of ZIF-8 and GO. The higher free volume, higher CO_2 adsorption, and lower crystallinity of MMMs enhanced the CO_2 permeability. The high porosity of ZIF-8 could increase the solubility selectivity, while the tortuous diffusion pathways created by GO nanosheets could increase the diffusivity selectivity. Chen *et al.*[19] synthesized ZIF-8@GO composite fillers with different reaction time by using the *in situ* growth method and incorporated it into a CO_2-philic, comb copolymer for the MMMs preparation. It was found that the reaction time of ZIF-8@GO plays a crucial role in improving the gas separation performance of MMMs. MMMs containing ZIF-8@GO synthesized from 6 h reaction time showed the highest CO_2 permeability of 475 barrer and CO_2/N_2 ideal selectivity of 58.2. Yang *et al.*[18] synthesized ZIF-8@GO composite fillers by continuously forming a ZIF-8 layer on the GO surface to overcome the stacking and folding issues of GO in MMMs. The prepared ZIF-8@GO composite fillers were incorporated into Pebax matrix to fabricate MMMs. The MMMs containing 20 wt% of ZIF-8@GO exhibited the best gas separation performance evidence by CO_2 permeability of 136.2 barrer and CO_2/N_2 ideal selectivity of 77.9. In comparison to the pristine Pebax membranes, the CO_2 permeability and CO_2/N_2 ideal selectivity increased by 66% and 60%, respectively. In comparison to the MMMs containing GO nanosheets, the CO_2 permeability increased by 75%, while the selectivity was not changed. It was found that the high porosity of ZIF-8 decreased the mass transfer resistance of GO by providing the transporting pathways around GO nanosheets for gas molecules, resulting in the increase of CO_2 permeability. The CO_2/N_2 selectivity was enhanced by abundant oxy-groups on GO surface.

According to the aforementioned literature survey, ZIF-8/GO composites have been intensively studied in the preparation of MMMs for gas separation.[17–19] The study of other MOF/GO composites is highly needed to explore the effects of MOF/GO composites on the gas separation performance of MMMs. MOFs consisting of the high-valence metal sites (Fe^{3+}) and the strong polarizing terephthalic acid can improve their molecular interaction with CO_2 molecules possessing quadrupole moment due to the electrical difference.[20] Moreover, the utilization of high-valence metal cation endows MOFs with high water-resistance. The nontoxic MIL-101 (Fe) showed higher adsorption capacity for CO_2 than N_2.[20] It was more often reported that the phase transition exists in the synthesis of the amino-functionalized NH_2-MIL-101 (Fe), comparing with the synthesis of MIL-101 (Fe).[21] However, this work intends to utilize the porous structure of MIL-101 (Fe) to provide additional pathways for gas molecules. The investigation of the crystal phase transition is not the focus of this work. MIL-101 (Fe)/GO has been used as catalyst and adsorbent for the water treatment processes.[22,23] To our best knowledge, it is the first time to synthesize MIL-101 (Fe)/GO composite fillers and investigate their effects on the membrane-based gas separation process. Therefore, MIL-101 (Fe)/GO composite fillers will be synthesized and incorporated into Pebax® 2533 matrix to prepare MMMs for CO_2/N_2 separation in this work.

2. Experimental

2.1. Materials

Ferric chloride hexahydrate ($FeCl_3 \cdot 6H_2O$), terephthalic acid (H_2BDC), *N*,*N*-dimethylformamide (DMF), and Graphene oxide powder (GO), 15–20 sheets, 4–10% edge-oxidized were purchased from Sigma Aldrich (Poznań, Poland). Methanol (99.8%) and ethanol (99.8%) were purchased from Alchem Grupa Sp. z o.o. (Toruń, Poland). Pebax® 2533 was kindly provided by Arkema (Colombes, France). Hydrophobic PVDF (polyvinylidene difluoride) membrane (Durapore Membrane Filter, 0.22 μm) were purchased from Merck (Darmstadt, Germany). CO_2 (99.999%) and N_2 (99.999%) were purchased from Air Products Sp. z o.o. (Siewierz, Poland).

2.2. Synthesis of MIL-101 (Fe) and MIL-GO fillers

MIL-101 (Fe) fillers were synthesized by using a solvothermal method.[22] 2.922 g ferric chloride hexahydrate and 0.854 g

terephthalic acid were dissolved in 60 mL DMF by stirring at room temperature for 1 h. Subsequently, the mixture solution was transferred into a Schott bottle and placed in oven at 120 °C for 24 hours. After cooling down to room temperature, the obtained composite fillers were collected by centrifugation and washed repeatedly with DMF and ethanol. Finally, the obtained composite fillers were dried in oven at 70 °C overnight and activated at 150 °C for 10 h.

To synthesize MIL-GO composite fillers, 1.461 g ferric chloride hexahydrate and 0.427 g terephthalic acid were dissolved in 30 mL DMF by stirring at room temperature for 1 h. Subsequently, a specific amount of GO was dispersed into 6 mL ethanol by using ultrasonic bath for half an hour. Then, the prepared GO dispersion was added into the above solution. After the complete mixing in the ultrasonic bath for half an hour, the mixture solution was transferred into Schott bottle and placed in oven at 120 °C for 24 hours. When the reaction is completed, the Schott bottle was cooled down to room temperature. The obtained composite fillers were collected by centrifugation and washed repeatedly with DMF and ethanol. Finally, the obtained composite fillers were dried in oven at 70 °C overnight and activated at 150 °C for 10 h. The content of GO in the composite filler was calculated by using the mass ratio of GO to GO, ferric chloride hexahydrate, and terephthalic acid. In this work, MIL-GO composite fillers containing 2 wt%, 5 wt%, and 10 wt% of GO were prepared and designated as MIL-GO-2, MIL-GO-5, and MIL-GO-10, respectively.

2.3. Membrane preparation

To prepare pristine Pebax® 2533/PVDF thin film membranes and MMMs, the casting solution of Pebax® 2533 solution (6 wt%) containing a specific amount of fillers were prepared firstly. The detailed procedure of the Pebax® 2533 solution preparation can be found elsewhere.[13] Pristine Pebax® 2533/PVDF membrane and MMMs were fabricated by casting a certain amount of the prepared solutions on the PVDF support by using the automatic film applicator. The casting knife with a 0.4 mm slit was used in this work. The casting speed is maintained at 10 mm s^{-1} for the preparation of all membranes. The freshly cast membranes were firstly dried at 25 °C for 24 h then further dried in an oven at 60 °C for 8 h to completely evaporate solvent. The composition of the selective layer, and the codes of the prepared membranes were listed in Table 1. In the nomenclature of the prepared membranes, P represents Pebax® 2533, M represents MIL-101 (Fe), G represents GO. For instance, 9-PMG2 presents Pebax-based MMMs containing 9.1 wt% MIL-GO-2 composite filler.

Table 1 Compositions and fabrication conditions of the prepared Pebax-based MMMs

	Composition of selective layer (wt%)		
Membrane	Pebax® 2533	Filler type	Filler content
Pebax® 2533/PVDF	100	—	0
9-PM/PVDF	90.9	MIL-101 (Fe)	9.1
9-PMG2/PVDF	90.9	MIL-GO-2	9.1
9-PMG5/PVDF	90.9	MIL-GO-5	9.1
9-PMG10/PVDF	90.9	MIL-GO-10	9.1
5-PMG2/PVDF	95.2	MIL-GO-2	4.8
13-PMG2/PVDF	87.0	MIL-GO-2	13.0

2.4. Material characterization

The morphologies of the synthesized MIL-101 (Fe), MIL-GO composite fillers and membranes were characterized by using Scanning Electron Microscope (SEM), LEO 1430 VP microscope (Leo Electron Microscopy Ltd, Cambridge, UK).

FTIR-ATR spectra of the synthesized MIL-101 (Fe), MIL-GO composite fillers and membranes were obtained by using Nicolet iS10 (Thermal Scientific, Waltham, USA) spectrometer in the range of 400–4000 cm^{-1}.

XRD analyses for the synthesized MIL-101 (Fe), and MIL-GO composite fillers were conducted by utilizing Philips X″Pert (Malvern Panalytical, Malvern, UK). The transmission mode and 2θ range of 5–80° were applied.

The nitrogen adsorption/desorption measurements for the synthesized MIL-101 (Fe), and MIL-GO composite fillers were conducted at −195.7 °C *via* Gemini VI (Micromeritics Instrument Corp., Norcross, GA, USA). All samples were degassed for 6 h at 110 °C before the measurements.

Thermal properties of the synthesized MIL-101 (Fe), MIL-GO composite fillers and membranes were analyzed by using a Jupiter STA 449 F5 (Netzsch, Germany) thermogravimetric analyzer. TGA measurements were conducted from 25 °C to 950 °C under the nitrogen atmosphere.

2.5. Gas permeation measurements

The gas permeation tests for pure gas of CO_2, and N_2, were conducted at 2–4 bar and 20 °C by using a home-made equipment (Fig. 1).[24] The effective membrane area in the module is 2.11 cm^2. Each membrane was measured 3 times for a better accuracy. The gas flow rate was recorded by using a bubble flow meter. The gas permeability P (1 barrer = 10^{-10} cm^3 (STP) cm cm^{-2} s^{-1} $cmHg^{-1}$) was calculated by using eqn (1):[16]

$$P = Ql/\Delta pA \quad (1)$$

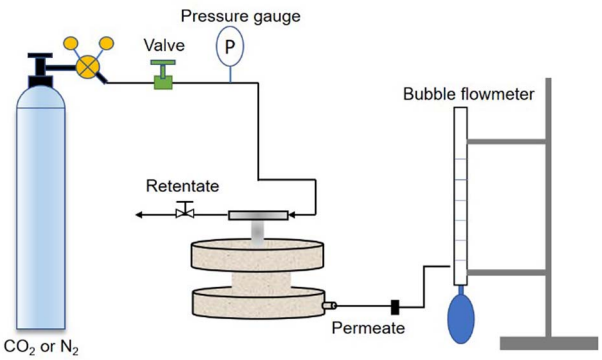

Fig. 1 The illustration of the laboratory permeation system for gas permeance measurements of flat sheet membranes.

where Q is the gas flow rate (cm^3(STP) s^{-1}); l is the membrane thickness (cm); Δp is the pressure difference across the membrane (cmHg); A is the active membrane area (cm^2).[4,16]

The ideal selectivity α_{12} was calculated by using eqn (2):[13]

$$\alpha_{12} = P1/P2 \quad (2)$$

3. Results and discussion

3.1. Characterization of MIL-101 (Fe) and MIL-GO fillers

SEM images of GO, MIL-101 (Fe), MIL-GO-2, MIL-GO-5, and MIL-GO-10 are shown in Fig. 2. The flakes of graphene sheets were observed for GO (Fig. 2(a and f)). MIL-101 (Fe) and MIL-GO-2 showed a regular octahedral structure (Fig. 2(b, c, g and h)). The crystal structure of MIL-101 (Fe) was perfectly preserved with addition of a small amount (2 wt%) of GO. However, with the increase of GO amount (5 and 10 wt%) in the MIL-GO composites, it can be clearly seen that the MIL-101 (Fe) particles possessing a spherical shape instead of the octahedral structure were formed on the GO sheets, which indicates the distortion of MIL-101 (Fe) crystals. The MIL-101 (Fe) crystal size in MIL-GO-5, and MIL-GO-10 composites is much smaller than that in pristine MIL-101 (Fe), and MIL-GO-2 composite (Fig. 2(d, e, i and j)). According to the estimation from SEM images, the MIL-101 (Fe) crystal size in pristine MIL-101 (Fe), and MIL-GO-2 composite is 0.6–1.0 μm, and 0.9–2.0 μm, respectively. While the MIL-101 (Fe) crystal size in MIL-GO-5, and MIL-GO-10 composites is 0.15–0.30 μm. This is because the GO sheets restrained the possible growth orientation of MIL-101 (Fe) crystal, which results in the formation of smaller and irregular MIL-101 (Fe) crystals on the surface of GO sheets.[22]

The XRD patterns of GO, MIL-101 (Fe), MIL-GO-2, MIL-GO-5, and MIL-GO-10 are presented in Fig. 3. The characteristic peaks of the synthesized MIL-101 (Fe) in the range of 5–25° were in good agreement with these of the previously reported MIL-101 (Fe),[22,25] indicating the good crystallinity of the prepared MIL-101 (Fe). Specifically, the observed peaks at 2 theta values of 5.81, 9.11, 9.50, 18.94, and 22.15° correspond to the (111), (220), (311), (511), and (825) crystal planes.[22] From the XRD patterns of MIL-GO-2, and MIL-GO-5, it can be seen the characteristic peaks of MIL-101 (Fe) were observed, while the intensity of the characteristic peaks of MIL-101 (Fe) decreased, indicating the crystal structure of MIL-101 (Fe) was preserved in at low content of GO. However, the characteristic peaks of MIL-101 (Fe) disappeared from the XRD pattern of MIL-GO-10. This is because the high GO content might limit the crystallization of MIL-101 (Fe) crystal and result in the distortion of MIL-101 (Fe) induced by the dispersed GO,[26,27] since most peaks from MIL-101 (Fe) disappeared except some new peaks produced in the composite filler and the peaks from GO (Fig. 3). Similar changes of XRD patterns were observed in MIL-88A(Fe)/GO,[27] and MOF-5/GO.[28] In this work, the characteristic peak for GO is at 2 theta value of 26° which represents (002) of the applied multi-layer GO with interlayer spacing of 0.336 nm according to the Bragg's law.[29] The typical characteristic peak of GO at 2 theta value of 10–12° was not observed since the amount of oxygen groups mainly located at the edges in the purchased GO sample is low.[30]

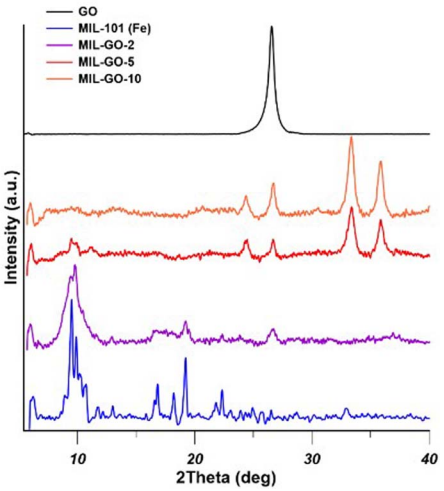

Fig. 3 XRD patterns of GO, MIL-101 (Fe), and MIL-GO fillers.

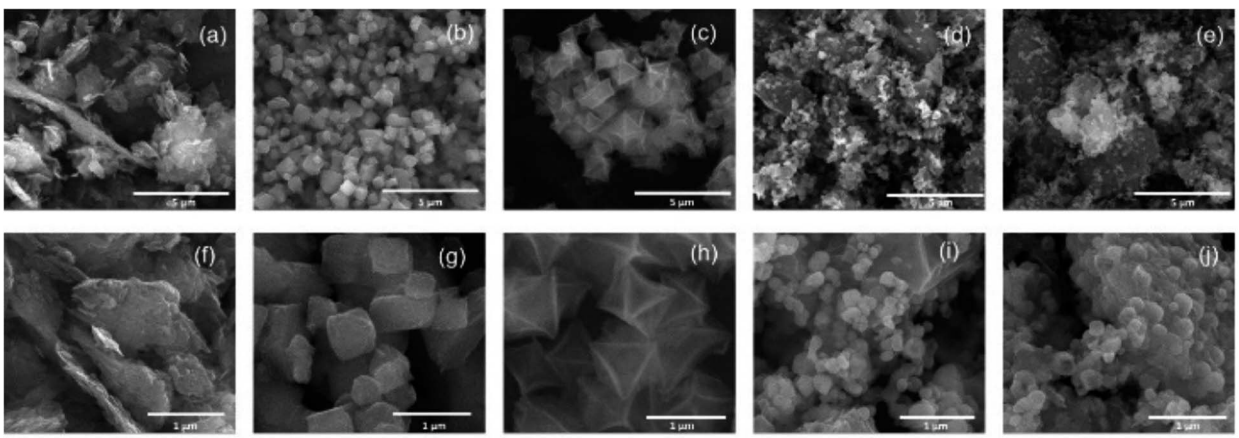

Fig. 2 SEM images of GO (a and f), MIL-101 (Fe) (b and g), MIL-GO-2 (c and h), MIL-GO-5 (d and i), and MIL-GO-10 (e and j).

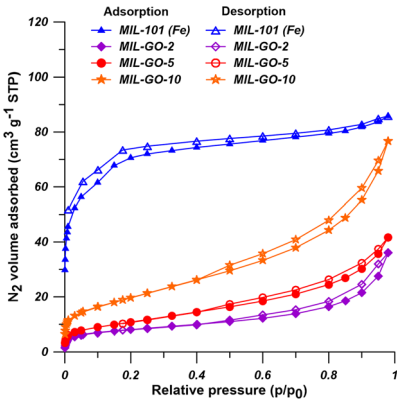

Fig. 4 N_2 adsorption/desorption isotherms of MIL-101 (Fe), MIL-GO-2, MIL-GO-5, and MIL-GO-10.

Fig. 4 and Table 2 show the N_2 adsorption/desorption isotherms and the textural properties of MIL-101 (Fe), MIL-GO-2, MIL-GO-5, and MIL-GO-10. According to IUPAC classification, the N_2 adsorption/desorption isotherms of the prepared MIL-101 (Fe) are ascribed to I-type adsorption isotherms indicating the presence of microporous structure in MIL-101 (Fe). While the N_2 adsorption/desorption isotherms of MIL-GO are assigned as II-type adsorption isotherms, implying the microporous and mesoporous structure in MIL-GO fillers.[31] The BET surface area of MIL-101 (Fe) is 239 m^2 g^{-1} which is comparable to the reported ones.[22,25] Liu *et al.*[22] and Zhao *et al.*[25] found that the BET surface area of MIL-101 (Fe) is 608 m^2 g^{-1} and 199 m^2 g^{-1}, respectively. Zorainy *et al.*[32] found the BET surface area of MIL-101 (Cr) and mixed-metal MIL-101(Cr/Fe) is over 2000 m^2 g^{-1}. Comparing with MIL-101 (Cr), the low BET surface area of the synthesized MIL-101 (Fe) could be attributed to the smaller crystal size of MIL-101 (Cr) than the synthesized MIL-101 (Fe). The texture properties and the crystal size of MIL-101 (Fe) are significantly influenced by the synthesis conditions.[21] In comparison to MIL-101 (Fe), the BET surface area, the total pore volume and the micropore volume decreased dramatically (Table 2), which can be ascribed to the coverage of MIL-101 (Fe) by nonporous GO sheets with low surface area.[33] Moreover, the mesopores were formed due to the addition of GO sheets in MIL-101 (Fe) synthesis process indicated by the presence of type H3 hysteresis loop in the N_2 adsorption/desorption isotherms of MIL-GO fillers.[34,35] It was noticed that the BET surface area and total pore volume of MIL-GO composite filler increased slightly when the GO content increased from 2 wt% to 10 wt%. Similar trend was observed by Liu *et al.*[27] In their work, the specific surface area of MIL-88A (Fe)/GO composite material increased with the increase of GO content since the addition of GO affects the crystallization process of MOF.[27]

Fig. 5 shows the TGA and DTG curves of GO, MIL-101 (Fe), and MIL-GO composites fillers. The total weight loss for GO is 8.6%, resulting from the decomposition of the epoxy groups and carboxylic groups, which indicated the high thermal stability of GO. For MIL-101 (Fe), the weight loss at 30–100 °C could be attributed to the evaporation of the adsorbed water and ethanol. The weight loss occurred at 100–350 °C due to the removal of DMF molecules and the free terephthalates in the pores of MIL-101 (Fe). Finally, the significant weight loss occurred from 350 °C to 760 °C, which could be resulted from the decomposition of the organic ligands, resulting in the collapse of the frameworks.[22,36] The MIL-GO composites fillers shared the similar thermal behavior with MIL-101 (Fe). Comparing to the total weight loss of 66% and the temperature of complete decomposition at 760 °C for MIL-101 (Fe), MIL-GO-2 exhibited the total weight loss of 67% and the temperature of complete decomposition at 720 °C. However, with the increase of the GO content in the MIL-GO composite fillers, the total weight loss decreased while the temperature of complete decomposition increased. MIL-GO-10 showed the highest temperature of complete decomposition of 975 °C, but the lowest total weight loss of 45%. It is found that the synthesized MIL-101 (Fe), and MIL-GO composites fillers showed high thermal stability. Moreover, the addition of GO can further increase their thermal stability.

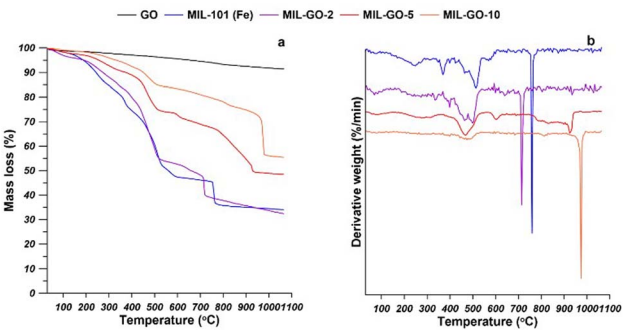

Fig. 5 TGA-DTG curves of GO, MIL-101 (Fe), and MIL-GO fillers.

Table 2 Textural properties of MIL-101 (Fe), MIL-GO-2, MIL-GO-5, and MIL-GO-10[a]

Samples	BET (m^2 g^{-1})	V_{Total} (cm^3 g^{-1})	V_{Micro} (cm^3 g^{-1})	V_{Meso} (cm^3 g^{-1})	Average pore diameter (nm)
MIL-101 (Fe)	239	0.186	0.109	0.077	1.24
MIL-GO-2	29	0.070	0.002	0.068	2.95
MIL-GO-5	40	0.076	0.004	0.072	3.31
MIL-GO-10	72	0.139	0.007	0.132	3.27

[a] V_{Micro}: micropore volume calculated by using the *t*-plot method. V_{Meso}: mesopore volume calculated from the subtraction of micropore volume from total pore volume.

The FTIR of GO, MIL-101 (Fe), and MIL-GO composites fillers are presented in Fig. 6. For GO, the peaks at 3400 cm^{-1}, 2120 cm^{-1}, and 1720 cm^{-1} could be related to the bands of –OH and C=O in carboxyl groups. The peak at 1618 cm^{-1} could be related to –OH in the absorbed water.[22] For MIL-101 (Fe) and MIL-GO composites fillers, the peak at 542 cm^{-1} was related to the Fe–O bond, and the peaks at 746 cm^{-1} and 1018 cm^{-1} were assigned to C–H bending in benzene and C–O–C vibration, respectively. Peaks at 1387 cm^{-1} and 1599 cm^{-1} could be originated from the symmetric and asymmetric vibrations of carboxyl bond (–COO–). The peak at 1653 cm^{-1} might be originated from the C=O bond in carboxyl group. The observed characteristic peaks for the synthesized MIL-101 (Fe) are in agreement with other reported literature.[22,23] The characteristic peaks of MIL-101 (Fe) were mostly found in the MIL-GO composite fillers, which indicates the successful formation of MIL-101 (Fe) with the presence of GO. However, the difference of IR spectra between MIL-101 (Fe) and MIL-GO composite can be observed. For example, the intensity of peak at 1653 cm^{-1} decreased as the GO content in MIL-GO composite increased. This is because the oxygen functional groups on GO surface can react with the carboxyl groups on MIL-101 (Fe), resulting in the reduction of C=O bonds of free carboxyl groups. The red shift of peaks 1599 cm^{-1} and 542 cm^{-1} was observed due to the interference of the GO characteristic peaks and the stronger interaction between MIL-101 (Fe) and GO.[23]

3.2. Characterization of MMMs

The morphology of cross-section and top surface of pristine Pebax® 2533 membrane and MMMs containing different types of fillers was shown by SEM images presented in Fig. 7. The surface of pristine Pebax® 2533 membrane is smooth while the surface became rough after the incorporation of MIL-101 (Fe) and MIL-GO composite fillers into the polymer matrix. However, the MMMs containing 9.1 wt% MIL-GO-2 and MIL-GO-5 possessed less rough surface than the MMMs containing 9.1 wt% MIL-101 (Fe) and MIL-GO-10, indicating the more desirable dispersion of MIL-GO-2 and MIL-GO-5 in polymer matrix. Most importantly, no defects were observed on the surfaces of all the prepared membrane. As shown in the cross-section of the prepared MMMs, there were no visible filler agglomeration nor voids at the interface between fillers and polymer matrix, which indicates the homogenous distribution of MIL-101 (Fe) and MIL-GO composite fillers in polymer matrix.

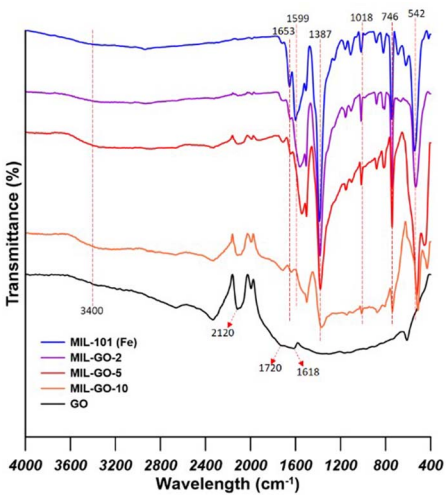

Fig. 6 FTIR spectra of GO, MIL-101 (Fe), and MIL-GO fillers.

The morphology of cross-section and top surface of pristine Pebax® 2533 membrane and MMMs containing different content of MIL-GO-2 composite filler was shown by SEM images presented in Fig. 8. The surfaces of MMMs became rougher with the increasing content of MIL-GO-2 composite filler. As shown in the cross-section of the prepared MMMs, the MIL-GO-2 composite fillers were dispersed homogeneously in polymer matrix at low filler content. No interfacial voids and visible agglomerates were observed. However, the filler agglomeration was observed when the filler content reached 13.0 wt%. Nevertheless, no interfacial voids were observed in the prepared MMMs.

The thermal properties of the prepared Pebax® 2533/PVDF MMMs were investigated by using TGA and DTG analysis. As it is shown in Fig. 9, the prepared MMMs exhibited similar TGA curves and the thermal weight loss rate curves, comparing to the pristine Pebax® 2533/PVDF membranes. Two main steps of weight loss were observed for the pristine Pebax® 2533/PVDF membranes and the prepared MMMs. The first step of weight loss occurred between 350 °C to 450 °C, which is resulted from the decomposition of polymer chains from Pebax® 2533.[24] The second step of weight loss occurred in the temperature range of 438 °C–500 °C, mainly due to the degradation of PVDF polymer chains.[37] It can be found that the incorporation of the prepared fillers into Pebax® 2533/PVDF composite MMMs did not change their thermal properties significantly. However, taking into consideration of the first DTG peak temperature which indicates the maximum rate of the weight loss in Pebax, it was found that the first DTG peak temperature increased from 415 °C for pristine Pebax® 2533/PVDF membranes to 425 °C–430 °C for the prepared MMMs containing 9 wt% of different types of fillers. MMMs containing 9 wt% of MIL-GO-2 composite filler showed the highest DTG peak temperature of 430 °C. It was also found the with the increase of MIL-GO-2 composite filler, the first DTG peak temperature increased. However, the second DTG peak temperature of MMMs remained the same as the pristine Pebax® 2533/PVDF membranes, since the prepared fillers were incorporated into the Pebax selective layer. The higher DTG peak temperature in the prepared MMMs indicated the slight enhancement of thermal stability of MMMs due to the limited thermal motion of polymer chains induced by the incorporated fillers.[17]

The FT-IR spectra of PVDF support, the pristine Pebax® 2533/PVDF thin film membranes and the prepared MMMs containing 9.1 wt% of MIL-101 (Fe), MIL-GO-2, MIL-GO-5, or MIL-GO-10 were shown in Fig. 10a. As can be seen, after the formation of Pebax selective layer on PVDF support, the characteristic peaks for PVDF disappeared, *e.g.*, the peaks at 1403 cm^{-1} corresponding to the C–H stretching vibration, 1181 cm^{-1}

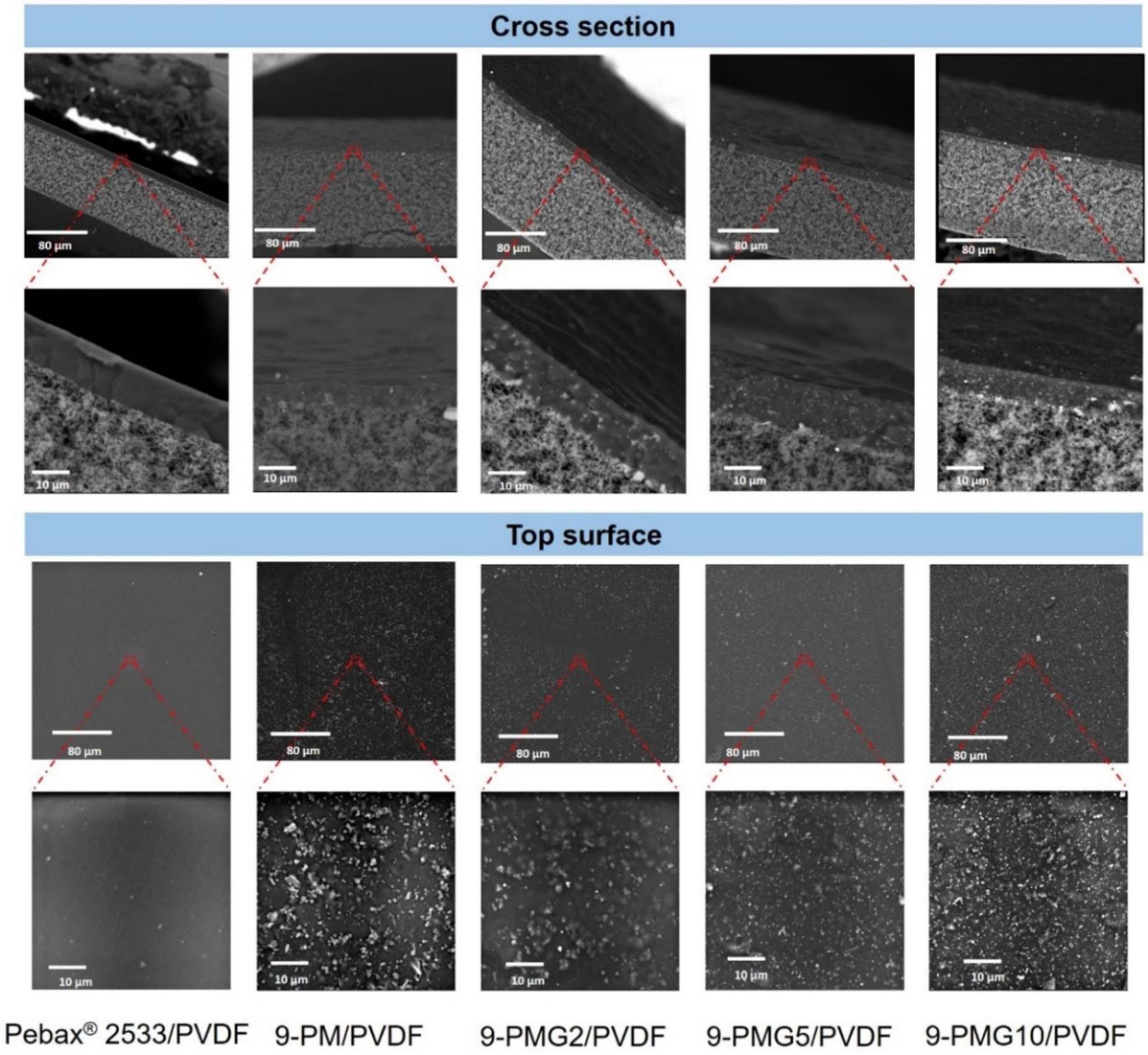

Fig. 7 SEM images of cross-section and surface of the pristine Pebax® 2533 membrane; MMMs with 9.1 wt% of MIL-101 (Fe); MIL-GO-2; MIL-GO-5; and MIL-GO-10, respectively.

and 1275 cm^{-1} corresponding to the stretching of C–F bonds,[38] and 764 cm^{-1} attributed to the bending of C–F bonds.[39] On the contrary, the characteristic peaks for Pebax were generated, *e.g.*, the peaks at 1109 cm^{-1} 3298 cm^{-1}, 1734 cm^{-1}, and 1640 cm^{-1} which were ascribed to the C–O–C bond from the PEO segment, the –N–H– stretching vibration, out-of-plane H–N–C=O vibration of amide, and O–C=O stretching vibration of carboxylic acid, respectively.[24] The peaks at 746 cm^{-1} and 1018 cm^{-1} which were related to the C–H bending in benzene and C–O–C vibration from MIL-101 (Fe) were generated in FT-IR spectra of the prepared MMMs. Moreover, with the increase of GO content in MIL-GO composite fillers, the intensity of the peak at 747 cm^{-1} corresponding to the C–H bending in benzene decreased, while the intensity of the peak at 1019 cm^{-1} corresponding to C–O–C vibration was the highest in MMMs containing MIL-GO-2 composite filler, which indicates the interaction between MIL-101 (Fe) and GO. These changes in intensity of peaks at 746 cm^{-1} and 1018 cm^{-1} observed from the FT-IR spectra for MMMs are consistent with that in the FT-IR spectra for the prepared fillers. The FT-IR spectra of the prepared MMMs containing various amount of MIL-GO-2 were presented in Fig. 10b. It was found that the intensity of characteristic peaks of MIL-GO-2 at 746 cm^{-1} and 1018 cm^{-1} increased with the increase of MIL-GO-2 composite filler content in MMMs.

3.3. Evaluation of gas separation performance of MMMs

3.3.1. The effect of filler types. Single gas permeation measurements were conducted to estimate the gas permeation performance of the prepared MMMs. In this study, permeability of pure gas (CO_2 and N_2) was determined at 2 bar and 20 °C. The effect of different fillers, *e.g.* MIL-101 (Fe), MIL-GO-2, MIL-GO-5, and MIL-GO-10 on the permeability of CO_2 and N_2, and the ideal selectivity of MMMs was shown in Fig. 11. It can be seen that the incorporation of fillers into Pebax® 2533 significantly

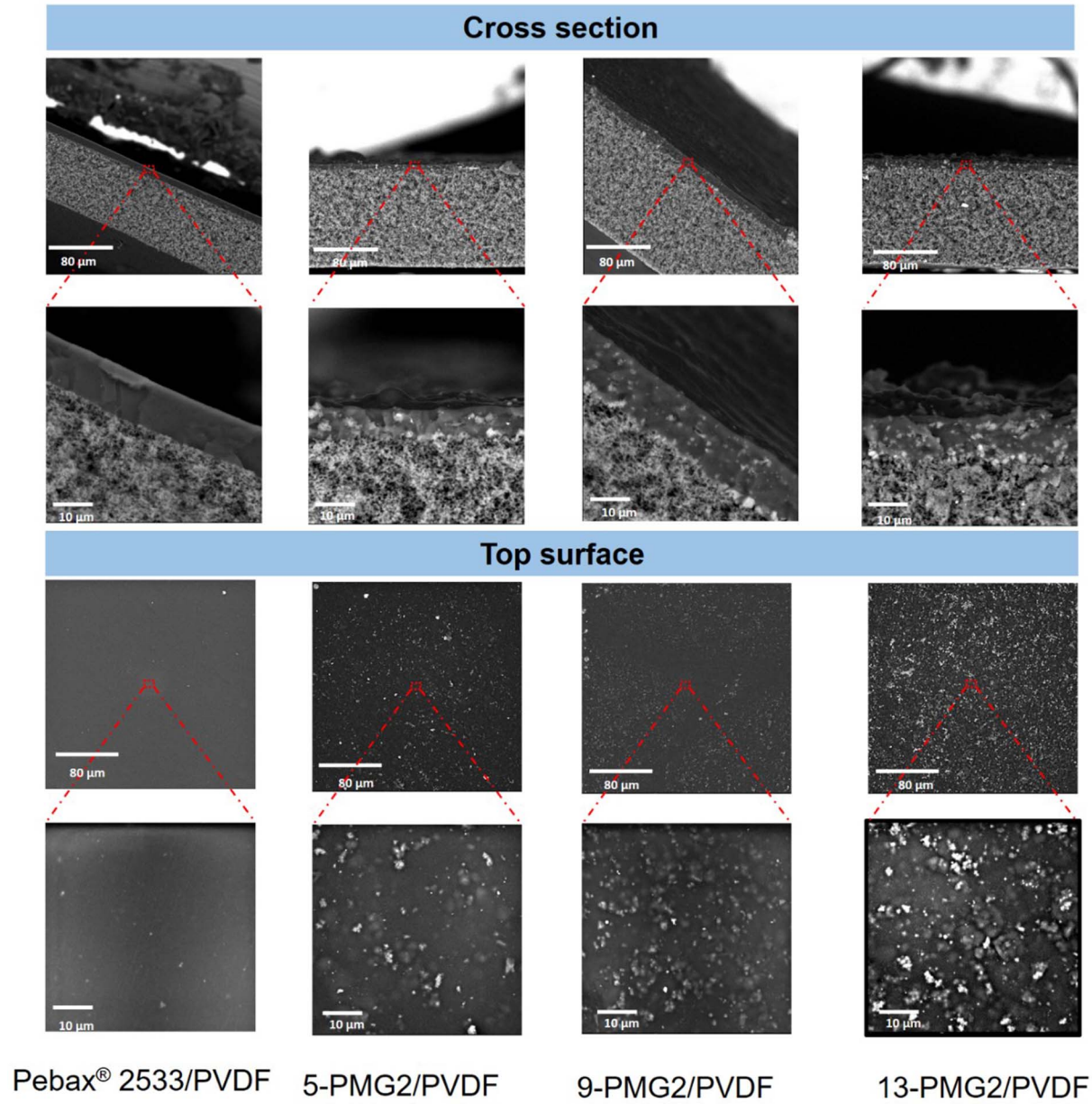

Fig. 8 SEM images of cross-section and surface of the pristine Pebax® 2533 membrane; MMMs with 4.8 wt%, 9.1 wt%, and 13.0 wt% of MIL-GO-2 composite filler.

influenced the gas transport properties of the prepared membranes. MMMs containing 9.1 wt% MIL-101 (Fe) exhibited CO_2 permeability equal to 323 barrer (1 barrer = 10^{-10} cm^3 (STP) cm cm^{-2} s^{-1} $cmHg^{-1}$) which is 59% higher than that of pristine Pebax membranes. While the CO_2/N_2 ideal selectivity equal to 17 was barely changed. The increase of CO_2 permeability can be explained by the following reasons. The incorporation of MIL-101 (Fe) disrupted the arrangement of polymer chains, resulting in the easier transport of gas molecules through membranes. Moreover, MIL-101 (Fe) provided additional free volume for gas molecules transport due to the high porosity and flexible framework of MIL-101 (Fe), which facilitated the transport of CO_2 through MMMs.[17,40] The ideal selectivity was slightly influenced after the incorporation of MIL-101 (Fe) due to the simultaneous enhancement of gas permeability of CO_2 and N_2, resulting from the porous structure and larger pore diameter (Table 2) than the diameter of CO_2 (0.33 nm) and N_2 (0.36 nm).

The incorporation of MIL-101 (Fe) into the Pebax® 2533 membranes has demonstrated the positive effect on the CO_2 permeability without the sacrifice of CO_2/N_2 ideal selectivity. To obtain the simultaneous enhancement of CO_2 permeability and CO_2/N_2 ideal selectivity, the MIL-GO composite fillers were synthesized and incorporated into Pebax® 2533 membranes due to the porous structure of MIL-101 (Fe) and high respect ratio of GO nanosheets. The effect of the mass ratio of GO to

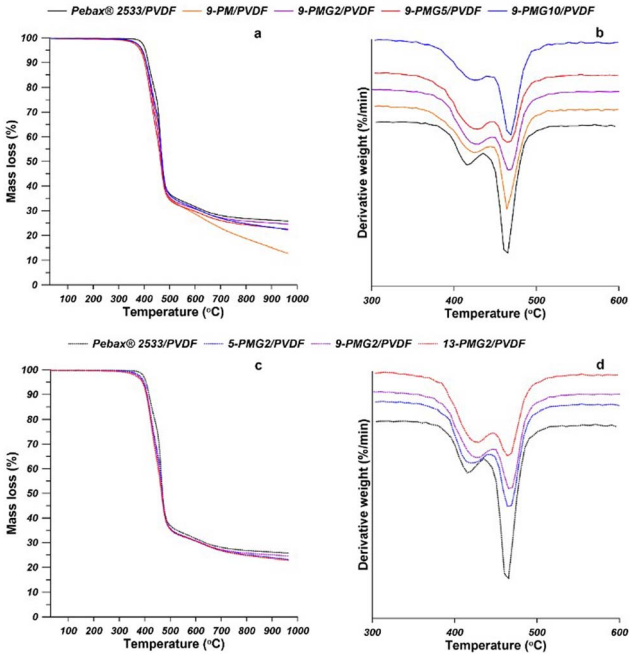

Fig. 9 TGA and DTG curves of MMMs containing 9 wt% of different types of fillers (a and b) and MMMs containing different content of MIL-GO-2 filler (c and d).

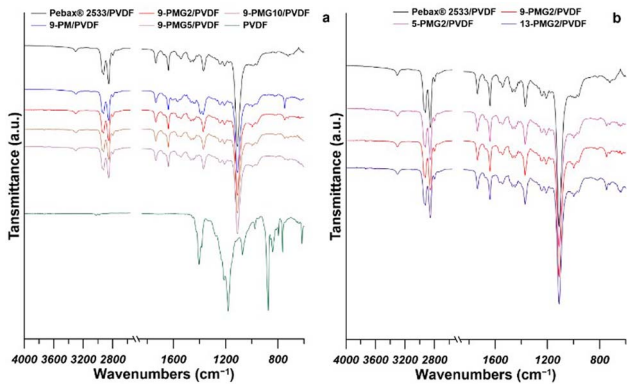

Fig. 10 FT-IR spectra of MMMs containing 9 wt% of different types of fillers (a) and MMMs containing different content of MIL-GO-2 filler (b).

MIL-GO composite filler on the gas permeation properties of MMMs was investigated by using the CO_2 permeability and CO_2/N_2 ideal selectivity of MMMs containing 9.1 wt% of MIL-GO-2, MIL-GO-5, or MIL-GO-10. It can be seen that the presence of MIL-GO-2 and MIL-GO-5 in MMMs showed enhancing effects on the CO_2 permeability and CO_2/N_2 ideal selectivity. On the contrary, the incorporation of MIL-GO-10 showed adverse effects on the gas separation properties of MMMs. In comparison to the pristine Pebax® 2533 membranes, the CO_2 permeability (equal to 303 barrer) of MMMs containing 9.1 wt% MIL-GO-2 was 50% higher. Moreover, the CO_2/N_2 ideal selectivity (equal to 24) of MMMs containing 9.1 wt% MIL-GO-2 was 41% higher than that of pristine Pebax® 2533 membranes and the highest among the prepared MMMs. However, the MMMs

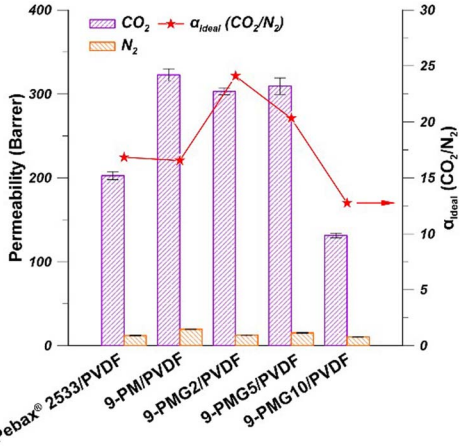

Fig. 11 Gas permeability and ideal selectivity of MMMs containing various types of fillers (filler content 9.1 wt%, experimental condition: 20 °C and 2 bar, the red line indicates only the trend of the ideal selectivity change).

containing 9.1 wt% MIL-GO-10 showed worse gas separation performance than that of pristine Pebax® 2533 membranes, evidenced by the lower CO_2 permeability (equal to 131 barrer) and the lower CO_2/N_2 ideal selectivity (equal to 13).

In order to account for the high CO_2 permeability and CO_2/N_2 ideal selectivity, it is crucial to elucidate the gas molecules transporting mechanism in MMMs containing MIL-GO-2 composite fillers. Solution diffusion model is mainly used as the transport mechanism for gas molecules in the prepared Pebax-based MMMs.[19,41] The incorporation of MIL-GO-2 composite filler into Pebax® 2533 membranes could affect the solubility and diffusivity of gas molecules in the prepared MMMs, resulting in the high CO_2 permeability and CO_2/N_2 ideal selectivity. First of all, the porous structure of MIL-101 (Fe) could increase the diffusion of gas molecules (CO_2 and N_2). Second, the incorporation of MIL-GO-2 could induce the additional free volume and the rearrangement of polymer chain packing in the MMMs, which facilitates the transport of gas molecules (CO_2 and N_2).[40] These two factors result in the enhancement of permeability of CO_2 and N_2 after the incorporation of MIL-GO-2 into Pebax® 2533 membranes (Fig. 11). However, the enhancement of CO_2 permeability was more significant than the enhancement of the N_2 permeability due to the smaller kinetic diameter of CO_2 (0.33 nm) than that of N_2 (0.36 nm). Third, the polar functional groups present in GO improved the affinity of CO_2 to MIL-GO-2 composite filler, which increased the solubility of CO_2 in MMMs due to the higher condensability of CO_2. The critical temperature of CO_2 (304.2 K) is higher than that of N_2 (126.1 K), resulting in higher condensability and solubility of CO_2 in MMMs.[19,42] Last but not least, the tortuous diffusion pathways were formed by GO nanosheets due to their high respect ratio, which significantly increased the diffusional resistance for larger N_2 molecules rather than smaller CO_2 molecules.[17,43] Moreover, the interdistance between GO nanosheets is 0.34 nm, which allowed the easier transport of smaller CO_2 molecules.[43] Based on the

above discussion on the effects of MIL-GO-2 on the gas molecules transporting mechanism in MMMs, the increased CO_2/N_2 ideal selectivity was mainly resulted from the synergistic effect of MIL-101 (Fe) and GO. The porous structure of MIL-GO-2, the additional free volume in MMMs and the higher affinity to CO_2 of MIL-GO-2 strongly enhanced the CO_2 permeability rather than N_2 permeability. The highly tortuous diffusion paths and the inter-distance between GO nanosheets inhibited the N_2 transport through MMMs. These factors collectively result in the increased CO_2/N_2 ideal selectivity.

When MIL-GO-10 containing higher GO ratio was incorporated into Pebax® 2533 membranes, the CO_2 permeability decreased dramatically and the N_2 permeability decreased slightly (Fig. 11). The reduction of gas permeability in MMMs containing MIL-GO-10 could be related to the decreased porosity and GO behavior of MIL-GO-10 composite filler. Casadei *et al.*[44] reported that the incorporation of GO into Pebax® 2533 membranes substantially decreased the permeability of CO_2 and N_2 since GO nanosheets created high tortuosity of diffusion path due to their high aspect ratio and low intrinsic permeability.[44] Moreover, it is reported that the stacked and folded morphology of GO sheets in MMMs could create the dead end zone and barrier structures, impairing the gas permeability.[18] According to the above discussion, the probable pathways of gas molecules in MMMs containing GO, MIL-101 (Fe) or MIL-GO composite fillers are visualized in Fig. 12.

3.3.2. The effect of MIL-GO-2 content. MMMs containing MIL-GO-2 demonstrated the best gas separation performance among the prepared MMMs. Therefore, the effect of MIL-GO-2 content on the gas permeability and ideal selectivity was investigated. As it is shown in Fig. 13, both the CO_2 permeability and CO_2/N_2 ideal selectivity have been significantly increased, while the N_2 permeability was not influenced when the MIL-GO-2 content increased to 9.1 wt%. MMMs containing 9.1 wt% MIL-GO-2 composite filler exhibited the highest CO_2 permeability equal to 303 barrer and CO_2/N_2 ideal selectivity equal to 24, which were 50% and 41% higher than those of pristine Pebax® 2533 membranes, respectively. The high gas separation performance of MMMs containing 9.1 wt% MIL-GO-2 composite filler was attributed to the multiple effects of the porous structure of MIL-GO-2, the additional free volume in MMMs, the higher affinity to CO_2 of MIL-GO-2, the highly tortuous diffusion paths and the inter-distance between GO nanosheets. More details about the analysis of gas transport

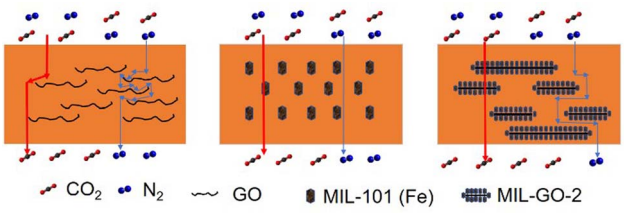

Fig. 12 Schematic diagram of the possible gas transport path in MMMs containing GO, MIL-101(Fe), or MIL-GO-2 composite fillers.

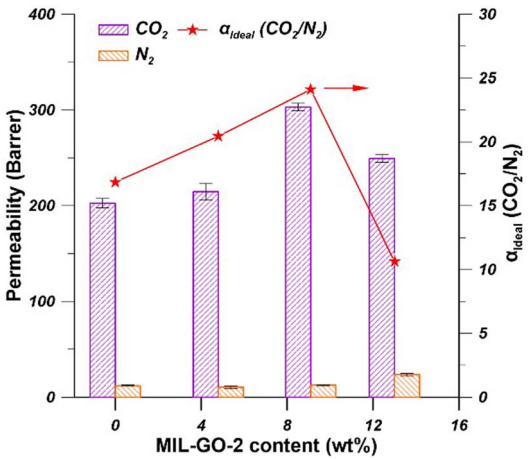

Fig. 13 Gas permeability and ideal selectivity of MMMs containing various amount of MIL-GO-2 (experimental condition: 20 °C and 2 bar).

mechanism in MMMs containing MIL-GO-2 composite filler can be found in Section 3.3.1. The further increase of MIL-GO-2 content in MMMs to 13.0 wt% resulted in the decrease of CO_2 permeability and CO_2/N_2 ideal selectivity. This could be related to the over-loading of MIL-GO-2, resulting in filler agglomeration and rigidified interface between filler and polymer chains.[43,45]

3.3.3. The effect of feed pressure. The effect of feed pressure on gas permeability and CO_2/N_2 ideal selectivity of pristine Pebax® 2533 membranes, MMMs containing 9.1 wt% MIL-101 (Fe), and MMMs containing 9.1 wt% MIL-GO-2 composite filler was also estimated. As shown in Fig. 14, the gas

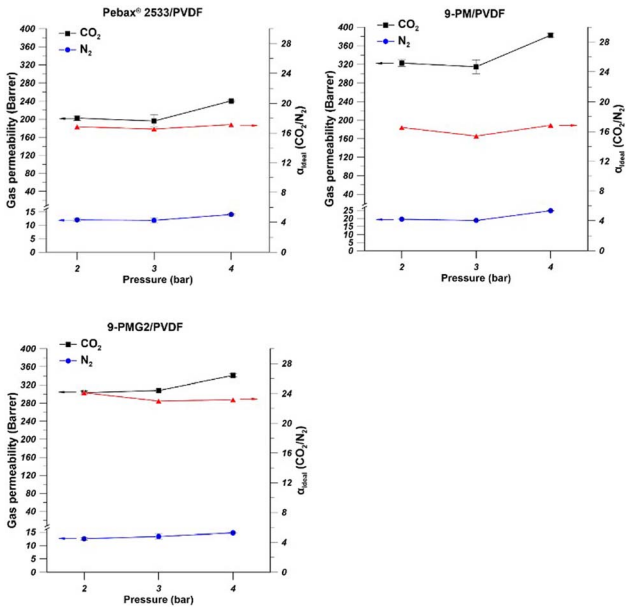

Fig. 14 Gas permeability and selectivity of pristine Pebax® 2533/PVDF membrane, MMMs containing 9.1 wt% of MIL-101 (Fe), and MMMs containing 9.1 wt% of MIL-GO-2 composite filler at various feed pressures.

permeability and CO_2/N_2 ideal selectivity of these three types of membranes exhibited the same behavior. When the feed pressure increased from 2 bar to 4 bar, the gas permeability of CO_2 and N_2 increased, while the CO_2/N_2 ideal selectivity was almost unchanged or slightly decreased. Similar results were reported by Guo *et al.*[46] In their research, ZIF-90@C_3N_4 composite filler was synthesized and incorporated into Pebax® 1657 membranes for CO_2/N_2 separation. It was found that both CO_2 permeability and N_2 permeability of MMMs containing 8 wt% ZIF-90@C_3N_4 increased to a certain extend when the feed pressure increased from 2 bar to 6 bar. The ideal selectivity was almost unchanged due to the high-efficiency screening capabilities of composite fillers.[46] In comparison to the N_2 permeability, CO_2 permeability was enhanced more significantly with the increase of feed pressure. This is because CO_2 possesses a smaller kinetic diameter (0.33 nm) and higher condensability.[19,42] In Pebax® 2533-based membranes, the solution-diffusion mechanism is the main separation principle. When the feed pressure increased, the solubility and diffusion rate of the gas molecules in membranes will increase, resulting in the increase of gas permeability.[46] Comparing the CO_2 permeability of these three types of membranes, it can be found that the increment of CO_2 permeability for MMMs containing 9.1 wt% MIL-GO-2 composite filler was less than that for the other two types of membranes. These results indicated that the performance of MMMs containing 9.1 wt% MIL-GO-2 composite filler was less sensitive to the feed pressure change.

3.3.4. Comparison with other Pebax-based MMMs reported in literature. The gas separation performance of the prepared MMMs in this work was comparable with other reported Pebax-based MMMs for CO_2/N_2 separation presented in Table 3. The prepared MIL-GO-2-Pebax® 2533/PVDF MMMs showed higher CO_2 permeability (303 barrer) than that of the reported Pebax-based MMMs containing singer filler (GO or MOFs),[40,43,47–51] along with the moderate CO_2/N_2 ideal selectivity (24). The moderate CO_2/N_2 ideal selectivity obtained in this work can be explained by the type of Pebax matrix. Pebax® 2533 consists of poly(ethylene oxide)-PEO block (80 wt%) and polyamide-PA block (20 wt%), while the Pebax® 1657 consists of poly(-ethylene oxide)-PEO block (60 wt%) and polyamide-PA block (40 wt%).[48,52] In comparison to the Pebax® 1657 membranes, the Pebax® 2533 membranes showed higher CO_2 permeability but lower CO_2/N_2 ideal selectivity due to the higher content of PEO block which possesses high mobility of polyether chains and strong affinity to CO_2 molecules.[52] Therefore, the reported Pebax® 1657-based MMMs showed relatively higher CO_2/N_2 ideal selectivity but relatively lower CO_2 permeability.[40,43,47–51] Taking into consideration the gas permeability and ideal selectivity, Pebax-based MMMs containing composite fillers[17,18,46,53] showed higher gas separation performance than those of the Pebax-based MMMs containing singer filler (GO or MOFs).[40,43,47–51] Therefore, the synthesis and utilization of 3D@2D composite filler demonstrated great potential in the preparation of high-performance MMMs for gas separation processes.

4. Conclusions

MIL-101 (Fe) and MIL-GO composites were successfully synthesized and used as fillers for the preparation of Pebax® 2533/PVDF thin film MMMs for CO_2/N_2 separation. The crystal structure of MIL-101 (Fe) and MIL-GO composites was confirmed by XRD pattern. Comparing with MIL-101 (Fe), the BET surface area and total pore volume of MIL-GO composites significantly decreased owing to the coverage of MIL-101 (Fe) by nonporous GO sheets with low surface area. The defect-free Pebax® 2533/PVDF thin film MMMs were successfully fabricated, indicating the homogeneous dispersion of the synthesized fillers in Pebax matrix. It was found that the incorporation of MIL-GO (Fe) into Pebax matrix significantly increased the

Table 3 Summary of gas separation performances of Pebax-based MMMs

Fillers	Filler content (wt%)	P_{CO_2} (barrer)	α_{CO_2/N_2}	Experimental condition: P (bar)/T (°C)	Ref.
MIL-53	10	129	48	10/35	47
NH_2-MIL-53	10	149	56	10/35	47
MIL-101	15	71	47	1.5/20	40
NH_2-MIL-101	5	74	43	1.5/20	40
UiO-66	7.5	90	60	3/20	48
ZIF-8	15	106	35	1/23	49
ZIF-7-CH_3OH	10	562	19	4.5/25	54
Zn/Ni-ZIF-8	15	440	40	2/25	55
ZIF-90@C_3N_4	8	110	84	2/25	46
GO	2	108	48	7/35	50
GO	2	100	68	2/30	51
GO	0.02	371	24	1/35	44
Reduced GO	5	119	104	2/30	43
MXene	1	148	63	2/30	51
ZIF-8@GO	6	249	47	1/25	17
ZIF-8@GO	20	136	78	3/25	18
CuBDC-ns@MoS_2	2.5	123	69	4/35	53
MIL-GO-2	9.1	303	24	2/20	This work

CO_2 permeability without changing the CO_2/N_2 ideal selectivity of Pebax selective layer. While the incorporation of MIL-GO-2 into Pebax matrix simultaneously increased the CO_2 permeability and the CO_2/N_2 ideal selectivity of Pebax selective layer. The improvement of the gas separation performance of MMMs resulted from the additional gas molecules pathway provided by MIL-GO-2, the additional free volume and the rearrangement of polymer chains in Pebax matrix, the high affinity of MIL-GO-2 to CO_2, and the tortuous diffusion pathways created by GO nanosheets. The prepared Pebax® 2533/PVDF thin film MMMs containing 9.1 wt% MIL-GO-2 demonstrated the highest CO_2 permeability equal to 303 barrer (1 barrer = 10^{-10} cm^3 (STP) cm cm^{-2} s^{-1} $cmHg^{-1}$) and the highest CO_2/N_2 ideal selectivity equal to 24.

Author contributions

Conceptualization, G. L. and W. K.; data curation, G. L. and K. K.; formal analysis, G. L., W. K., K. K. and J. K.; funding acquisition, G. L. and W. K.; investigation, G. L.; methodology, G. L., W. K. and J. K.; resources, W. K.; software, K. K. and J. K.; supervision, W. K. and J. K.; validation, G. L.; visualization, G. L. and K. K.; writing—original draft, G. L.; writing—review & editing, G. L., W. K. and K. K. All authors have read and agreed to the published version of the manuscript.

Conflicts of interest

There are no conflicts to declare.

Acknowledgements

This work was supported by the fund from Excellence Initiative – Research University – Nicolaus Copernicus University in Torun (Emerging Field and Grants4NCUStudents).

Notes and references

1 Q. Sohaib, A. Muhammad, M. Younas and M. Rezakazemi, *Sep. Purif. Technol.*, 2020, **241**, 116677.
2 N. Hajilary, M. Rezakazemi and A. Shahi, *Mater. Sci. Energy Technol.*, 2020, **3**, 218–224.
3 A. Arabi Shamsabadi, M. Rezakazemi, F. Seidi, H. Riazi, T. Aminabhavi and M. Soroush, *Prog. Energy Combust. Sci.*, 2021, **84**, 100903.
4 C. Ma, M. Wang, Z. Wang, M. Gao and J. Wang, *J. CO2 Util.*, 2020, **42**, 101296.
5 S. Bandehali, A. Moghadassi, F. Parvizian, S. M. Hosseini, T. Matsuura and E. Joudaki, *J. Energy Chem.*, 2020, **46**, 30–52.
6 H. Rajati, A. H. Navarchian, D. Rodrigue and S. Tangestaninejad, *Chem. Eng. Process.*, 2021, **168**, 108590.
7 L. M. Robeson, *J. Membr. Sci.*, 2008, **320**, 390–400.
8 A. R. Kamble, C. M. Patel and Z. V. P. Murthy, *Renewable Sustainable Energy Rev.*, 2021, **145**, 111062.
9 M. M. Zagho, M. K. Hassan, M. Khraisheh, M. A. A. Al-Maadeed and S. Nazarenko, *Chem. Eng. J. Adv.*, 2021, **6**, 100091.
10 M. M. H. Shah Buddin and A. L. Ahmad, *J. CO2 Util.*, 2021, **51**, 101616.
11 M. Vinoba, M. Bhagiyalakshmi, Y. Alqaheem, A. A. Alomair, A. Pérez and M. S. Rana, *Sep. Purif. Technol.*, 2017, **188**, 431–450.
12 S. S. Swain, L. Unnikrishnan, S. Mohanty and S. K. Nayak, *Int. J. Hydrogen Energy*, 2017, **42**, 29283–29299.
13 G. Li, W. Kujawski, K. Knozowska and J. Kujawa, *Materials*, 2021, **14**, 3366.
14 W. Chen, Z. Zhang, C. Yang, J. Liu, H. Shen, K. Yang and Z. Wang, *J. Membr. Sci.*, 2021, **636**, 119581.
15 Y. Shi, S. Wu, Z. Wang, X. Bi, M. Huang, Y. Zhang and J. Jin, *Sep. Purif. Technol.*, 2021, **277**, 119449.
16 C. Jiao, Z. Li, X. Li, M. Wu and H. Jiang, *Sep. Purif. Technol.*, 2021, **259**, 118190.
17 L. Dong, M. Chen, J. Li, D. Shi, W. Dong, X. Li and Y. Bai, *J. Membr. Sci.*, 2016, **520**, 801–811.
18 K. Yang, Y. Dai, X. Ruan, W. Zheng, X. Yang, R. Ding and G. He, *J. Membr. Sci.*, 2020, **601**, 117934.
19 B. Chen, C. Wan, X. Kang, M. Chen, C. Zhang, Y. Bai and L. Dong, *Sep. Purif. Technol.*, 2019, **223**, 113–122.
20 H. R. Mahdipoor, R. Halladj, E. Ganji Babakhani, S. Amjad-Iranagh and J. Sadeghzadeh Ahari, *Colloids Surf., A*, 2021, **619**, 126554.
21 M. Y. Zorainy, M. Gar Alalm, S. Kaliaguine and D. C. Boffito, *J. Mater. Chem. A*, 2021, **9**, 22159–22217.
22 Z. Liu, W. He, Q. Zhang, H. Shapour and M. F. Bakhtari, *ACS Omega*, 2021, **6**, 4597–4608.
23 J. Lin, H. Hu, N. Gao, J. Ye, Y. Chen and H. Ou, *J. Water Process. Eng.*, 2020, **33**, 101010.
24 G. Li, W. Kujawski, A. Tonkonogovas, K. Knozowska, J. Kujawa, E. Olewnik-Kruszkowska, N. Pedišius and A. Stankevičius, *Chem. Eng. Res. Des.*, 2022, **181**, 195–208.
25 F. Zhao, Y. Liu, S. B. Hammouda, B. Doshi, N. Guijarro, X. Min, C.-J. Tang, M. Sillanpää, K. Sivula and S. Wang, *Appl. Catal., B*, 2020, **272**, 119033.
26 C. Petit and T. J. Bandosz, *Adv. Funct. Mater.*, 2011, **21**, 2108–2117.
27 N. Liu, W. Huang, X. Zhang, L. Tang, L. Wang, Y. Wang and M. Wu, *Appl. Catal., B*, 2018, **221**, 119–128.
28 C. Petit and T. J. Bandosz, *Adv. Mater.*, 2009, **21**, 4753–4757.
29 M. Seredych, C. Petit, A. V. Tamashausky and T. J. Bandosz, *Carbon*, 2009, **47**, 445–456.
30 F. Besharat, M. Manteghian, G. Gallone and A. Lazzeri, *Nanotechnology*, 2020, **31**, 155701.
31 M. D. Donohue and G. L. Aranovich, *Adv. Colloid Interface Sci.*, 1998, **76–77**, 137–152.
32 M. Y. Zorainy, H. M. Titi, S. Kaliaguine and D. C. Boffito, *Dalton Trans.*, 2022, **51**, 3280–3294.
33 C. Yang, X. You, J. Cheng, H. Zheng and Y. Chen, *Appl. Catal., B*, 2017, **200**, 673–680.
34 J. Zhu, H. Zhang, Q. Liu, C. Wang, Z. Sun, R. Li, P. Liu, M. Zhang and J. Wang, *J. Taiwan Inst. Chem. Eng.*, 2019, **99**, 45–52.
35 K. S. W. Sing and R. T. Williams, *Adsorpt. Sci. Technol.*, 2004, **22**, 773–782.

36 M.-L. Chen, S.-Y. Zhou, Z. Xu, L. Ding and Y.-H. Cheng, *Molecules*, 2019, **24**, 3718.
37 W. Li, H. Li and Y.-M. Zhang, *J. Mater. Sci.*, 2009, **44**, 2977–2984.
38 Z. Zeng, D. Yu, Z. He, J. Liu, F.-X. Xiao, Y. Zhang, R. Wang, D. Bhattacharyya and T. T. Y. Tan, *Sci. Rep.*, 2016, **6**, 20142.
39 S. Govender, W. Przybylowicz and P. Swart, *Desalin. Water Treat.*, 2009, **9**, 272–278.
40 C. Song, R. Li, Z. Fan, Q. Liu, B. Zhang and Y. Kitamura, *Sep. Purif. Technol.*, 2020, **238**, 116500.
41 J. G. Wijmans and R. W. Baker, *J. Membr. Sci.*, 1995, **107**, 1–21.
42 Q. Xin, Z. Li, C. Li, S. Wang, Z. Jiang, H. Wu, Y. Zhang, J. Yang and X. Cao, *J. Mater. Chem. A*, 2015, **3**, 6629–6641.
43 G. Dong, J. Hou, J. Wang, Y. Zhang, V. Chen and J. Liu, *J. Membr. Sci.*, 2016, **520**, 860–868.
44 R. Casadei, M. Giacinti Baschetti, M. J. Yoo, H. B. Park and L. Giorgini, *Membranes*, 2020, **10**, 188.
45 S. Khoshhal Salestan, K. Pirzadeh, A. Rahimpour and R. Abedini, *J. Environ. Chem. Eng.*, 2021, **9**, 105820.
46 F. Guo, D. Li, R. Ding, J. Gao, X. Ruan, X. Jiang, G. He and W. Xiao, *Sep. Purif. Technol.*, 2022, **280**, 119803.
47 S. Meshkat, S. Kaliaguine and D. Rodrigue, *Sep. Purif. Technol.*, 2018, **200**, 177–190.
48 J. Shen, G. Liu, K. Huang, Q. Li, K. Guan, Y. Li and W. Jin, *J. Membr. Sci.*, 2016, **513**, 155–165.
49 M. Li, X. Zhang, S. Zeng, L. bai, H. Gao, J. Deng, Q. Yang and S. Zhang, *RSC Adv.*, 2017, **7**, 6422–6431.
50 D. Zhao, J. Ren, Y. Qiu, H. Li, K. Hua, X. Li and M. Deng, *J. Appl. Polym. Sci.*, 2015, **132**, 42624.
51 F. Shi, J. Sun, J. Wang, M. Liu, Z. Yan, B. Zhu, Y. Li and X. Cao, *J. Membr. Sci.*, 2021, **620**, 118850.
52 L. Liu, A. Chakma and X. Feng, *Ind. Eng. Chem. Res.*, 2005, **44**, 6874–6882.
53 N. Liu, J. Cheng, W. Hou, C. Yang, X. Yang and J. Zhou, *Sep. Purif. Technol.*, 2022, **282**, 120007.
54 J. Gao, H. Mao, H. Jin, C. Chen, A. Feldhoff and Y. Li, *Microporous Mesoporous Mater.*, 2020, **297**, 110030.
55 X. Zhang, T. Zhang, Y. Wang, J. Li, C. Liu, N. Li and J. Liao, *J. Membr. Sci.*, 2018, **560**, 38–46.